UDC 621.3 https://doi.org/10.20998/2074-272X.2025.6.10

S.E. Rezgui, Z. Darsouni, H. Benalla

Nonlinear vector control of multiphase induction motor using linear quadratic regulator and active disturbances rejection control under disturbances and parameter variations

Introduction. *This paper introduces a hybrid control strategy for multiphase induction motors, specifically focusing on the dual star induction motor (DSIM) by integrating active disturbances rejection control (ADRC) and linear quadratic regulator (LQR).* ***Problem.*** *Conventional PI-based indirect field oriented control (IFOC) of DSIM drives exhibit 3 critical shortcomings: 1) sensitivity to parameter variations, such as rotor resistance fluctuations; 2) sluggish transient response during rapid speed and torque changes; 3) slow disturbances rejection, such as sudden load torque variations. The* ***goal*** *of this work is to achieve enhanced reliability, precision and robustness of DSIM drives in high-performance demand applications such as automotive.* ***Methodology.*** *The proposed hybrid control architecture is structured as follows: 1) IFOC decoupling. The DSIM's stator currents are decomposed into 2 components using Park transformations, aligning the rotor flux vector to the d-axis. 2) The LQR is designed to optimize the outer speed/torque loop regulation by minimizing control efforts and state deviations. 3) ADRCs controllers are designed in the inner current loops. Each controller utilizes an extended state observer to estimate and compensate parameter variations and external disturbances in real time.* ***Results.*** *Simulations using MATLAB/Simulink validation on a 5 kW DSIM under multiple scenarios confirm the robustness of the proposed hybrid strategy.* ***Scientific novelty.*** *The contribution lies in the integration of ADRC and LQR in IFOC: The hierarchical fusion of ADRC (inner loops) and LQR (outer loop) uniquely leverages ADRC's and the LQR's real-time power to handle any disturbances and unmodeled dynamics.* ***Practical value.*** *The proposed technique demonstrates enhanced performances in speed's response, sudden load torque demands and parameter variations. It exhibited high robustness even under degraded conditions such as phase faults, making this strategy ideal for high-performance applications like electric vehicles, where stability and adaptability are critical.* References 31, tables 2, figures 24.

Key words: **optimal control, active disturbances rejection control, indirect field-oriented control, multiphase induction motor, three-level neutral point clamped inverters.**

Вступ. *У статті розглядається гібридна стратегія управління багатофазними асинхронними двигунами, зокрема з фокусом на асинхронний двигун з подвійною зіркою (DSIM),шляхом залучення активного управління придушенням збурень (ADRC) та лінійно-квадратичного регулятора (LQR).* ***Проблема***. *Традиційне непряме полеорієнтоване управління (IFOC) на основі ПІ-регулятора приводів DSIM має 3 критичні недоліки: 1) чутливість до змін параметрів, таких як коливання опору ротора; 2) інерційний перехідний процес при швидких змінах швидкості та крутного моменту; 3) повільне придушення збурень, таких як різкі зміни крутного моменту навантаження.* ***Метою*** *роботи є підвищення надійності, точності та стійкості приводів DSIM у високопродуктивних застосуваннях, таких як автомобілебудування.* ***Методологія***. *Запропонована архітектура гібридного управління структурована таким чином: 1) Розв'язування IFOC. Струми статора DSIM розкладаються на 2 складові з використанням перетворень Парка, вирівнюючи вектор потоку ротора осі d. 2) LQR призначений для оптимізації регулювання зовнішнього контуру швидкості/крутного моменту за рахунок мінімізації зусиль з управління та відхилень стану. 3) Контролери ADRC спроєктовані у внутрішніх струмових контурах. Кожен контролер використовує розширений спостерігач стану для оцінки та компенсації змін параметрів та зовнішніх збурень у реальному часі.* ***Результати***. *Моделювання з використанням валідації у MATLAB/Simulink для 5 кВт DSIM у кількох сценаріях підтверджує надійність запропонованої гібридної стратегії.* ***Наукова новизна***. *Внесок полягає в інтеграції ADRC і LQR в IFOC: ієрархічне злиття ADRC (внутрішніх контурів) і LQR (зовнішнього контуру) унікальним чином використовує потужність ADRC та LQR в реальному часі для обробки будь-яких збурень та немодельованої динаміки.* ***Практична цінність***. *Запропонована методика демонструє покращені характеристики при реагуванні на швидкість, раптові вимоги до крутного моменту навантаження і зміни параметрів. Він показав високу надійність навіть за умов погіршення характеристик, таких як фазові замикання, що робить цю стратегію ідеальною для високопродуктивних застосувань, таких як електромобілі, де стабільність та адаптивність мають вирішальне значення.* Бібл. 31, табл. 2, рис. 24.

Ключові слова: **оптимальне керування, активне придушення перешкод, опосередковане полеорієнтоване керування, багатофазний асинхронний двигун, трирівневі інвертори з фіксованою нейтральною точкою.**

Introduction. Three-phase induction motors have broad applications across industries and electric traction and have gained large attention in recent researches [1, 2]. However, multiphase motors have become favored in traction applications like electric vehicles and electric marine propulsion due to their superior features over three-phase motors. They distribute power across more phases, reducing power per phase and torque ripples. Multiphase motors enhance fault tolerance and torque density with increased degrees of freedom and harmonic current reduction [3]. However, multiphase motors are inherently nonlinear systems due to their coupling between stator and rotor flux dynamics. As a result, achieving precise control over their dynamic performance during variations in speed and torque remains a challenging task. The choice of strategy depends on the specific application, computational resources, and performance requirements. To this end, innumerable control strategies have been developed to fully exploit multiphase induction motors performance across various operating points.

Starting with the most familiar strategies, namely scalar control, vector control, and direct torque control (DTC) [4–8], where authors [5] designed a flux and speed state observer for sensorless control of a dual star induction motor (DSIM) for direct vector control. A comparison with the sliding mode model reference adaptive system technique was conducted to evaluate speed and flux tracking during transients and parameter variations. The results demonstrated the observer's superior robustness against uncertainties, disturbances, and speed changes, while reducing torque ripple compared to model reference adaptive system. However, the proposed state observer still sensitive to parameters variations particularly in low speed. A novel vector control scheme for speed sensorless control of a dual stator induction generator in a grid-connected wind energy conversion system is presented in [6]. This work introduced a 9-zone space vector-based hybrid pulse width modulation (PWM), which optimally controlled

grid and motor side converters, reducing torque pulsation, current ripple, and switching losses. Simulation and laboratory validation demonstrated that the proposed sensorless control outperformed conventional vector control schemes. However, while the hybrid PWM and sensorless control provide significant advantages, the work lacks parameter variation tests.

When conventional DTC scheme is extended for the multiphase motors, it can produce undesirable harmonics (5^{th} and 7^{th} order) in phase currents which cause losses in the motor winding, as a remedy, a simplified method of synthetic vectors generation is proposed in [7]. By using the mapped voltage vectors in *d-q* and *x-y* subspaces, dwell times are calculated to suppress the effect of some undesirable vectors and generate new synthetic vectors. These latter are achieved by both field programmable gate array and PWM module. Experimental results shown that with the proposed DTC the current's total harmonic distortion (THD) is reduced by ≈70 % when compared to that of traditional structure. The authors [8] proposed a modified DTC strategy that employs a 2-step approach to select the optimal vector for supplying the DSIM, effectively reducing harmonic currents. To address the steady-state torque error associated with the conventional 5-level hysteresis controller, they developed a 5-level torque regulator that replaces the zero-voltage vector with active voltage vectors and incorporates a PI controller within its structure to enhance steady-state performance.

More advanced techniques have been investigated, for instance, in [9], the authors presented a sensorless control system using super twisting sliding mode control for direct speed and flux control, which ensured robustness, finite-time convergence, and reduced chattering while eliminating speed and position sensors. The innovative torque-sharing algorithm enhanced performance across a wide speed range, including zero speed, preventing winding overload. However, the dependency on the observer of the rotor speed and winding fluxes was a notable problem, along with the need for load torque information for optimal torque sharing. Following the SMC context, authors [10] proposed a nonlinear integral backstepping control for DSIM, improving robustness under parameter variations by using both reduced and complete mathematical models. The control strategy ensured asymptotic global stability and effective load disturbance rejection. Simulation results validated the superiority of the complete model over the reduced one, showing better handling of internal parameter changes, particularly rotor resistance, maintaining decoupling between flux and torque. However, the increased complexity in implementing the complete model was a drawback compared to the simpler reduced model.

Model predictive control has gained a lot of interest from the AC motors control community due to its effectiveness in controlling multi-input, multi-output systems with constraints. Several enhanced model predictive control strategies have been developed with the aim of exploring more efficient solutions [11, 12]. The objectives include simplifying algorithms, designing optimal weighting factors, improving parameter robustness, and minimizing current or torque ripples. For example, in [13], the authors proposed a new modulation strategy in model predictive currents control (MPCC) that combines virtual vectors and space vector modulation for an asymmetrical 6-phase induction motor. Compared to previous MPCC strategies, such as MPCC with virtual vectors and MPCC with finite set formulation, the proposed MPCC outperforms these methods in *x-y* current reduction and THD. Additionally, a robustness test confirmed the controller's stability under parameter variations.

Some works have been devoted to model reference adaptive control techniques for the DSIM speed control. An adaptive control technique based on the Landau stability theorem was applied in [14] to improve speed regulation. The controller adapts parameters over time using a closed-loop output error algorithm, ensuring robustness against motor parameter variations. Simulation results demonstrated satisfactory speed control, quick disturbance rejection, and smooth electromagnetic torque without peaks. Robustness tests under rotor resistance variations confirmed the method's efficiency in normal and severe conditions.

Other papers have opted to use AI-based strategies as fuzzy, neural network and neuro-fuzzy controllers. An adaptive fuzzy controller based on Lyapunov's stability algorithm was developed in [15]. The approach used a recalculation of the PI-fuzzy speed gains regulator in real time. MATLAB/Simulink simulations showed improved tracking performance and robustness against parameter variations compared to the conventional PI-fuzzy controller. However, tests were limited to medium speeds (±100 rad/s), the DSIM was not at full load, and keeping traditional PI current controllers make the system susceptible to disturbances. A sensorless 5-level DTC scheme based on neural networks and an extended Kalman filter for a DSIM was studied in [16]. To improve robustness and dynamic performance, artificial neural networks were employed, and extended Kalman filter was used to estimate rotor speed, reducing sensor requirements and installation costs. Simulation results in MATLAB demonstrated that the proposed control scheme provided highly satisfactory performance for the DSIM. However, the work necessitates tests at low speeds as well as evaluations of robustness against parameter variations. In [17], a neuro-fuzzy scheme was developed for speed control of a DSIM with improved performance. A 4-layer network was used to optimize the fuzzy elements by minimizing the squared error. Two 5-level inverters with PWM techniques and indirect field-oriented control (IFOC) were implemented. Simulation results showed the neuro-fuzzy controller provided better speed response, robustness to load disturbances, and parameter variations compared to a conventional inverter. Additionally, the 5-level inverter significantly reduced stator currents and pulsating electromagnetic torque. Another aspect of AI optimization techniques has been used with a synergetic control to improve the performance of vector control scheme of a DSIM in [18]. The optimal parameters in the speed loop are obtained based on the synergistic control theory and the particle swarm optimization. The results showed that synergetic control enhances the robustness of drive speed control, offering superior performance in load torque rejection and reducing torque vibrations caused by chattering.

Optimal control strategies, like the linear quadratic regulator (LQR), aim to minimize a defined cost function, such as energy consumption, torque ripple, or trajectory tracking errors, while adhering to system constraints. Although these techniques are not commonly applied to

multiphase motors, studies in [19–21] investigated their use for induction motors, showing promising potential for such strategies.

Finally, in [22], the authors proposed a control scheme for a DSIM using active disturbance rejection control (ADRC) without relying on current or speed sensors. By utilizing only DC voltage information and the switching states of the converters, voltage observers were employed to estimate the stator currents and rotor speed. It is noteworthy that ADRC was applied solely to the stator currents, while traditional PI controllers were retained for speed and flux control. However, despite the promising results, the system was not tested under conditions of parameter variation.

To ensure high robustness against external disturbances, such as load torque variations and changes in speed reference, and to improve the efficiency of the IFOC system in addressing internal disturbances, including variations in stator and rotor resistance as well as changes in the moment of inertia and even in degraded conditions such as phase fault, 2 advanced regulators will be utilized. The LQR regulator will be employed to regulate speed and torque, while the ADRC regulator will be used to control the reference voltages of the inverters. By adopting this approach, classical PI regulators will be avoided, thereby eliminating the performance limitations typically associated with these regulators.

The main problem addressed is: how can a hybrid LQR-ADRC strategy be designed and validated to replace conventional PI regulators in IFOC systems, ensuring superior robustness, efficiency, and fault tolerance under complex operational scenarios? By resolving this, the study aims to eliminate the performance limitations of PI-based systems while enhancing the reliability of multiphase motor drives in electric vehicles.

Mathematical methods and modeling.

Model of the DSIM. The DSIM is a type of a 3-phase induction motors which contain dual stators coupled in star, the phase shift between the first and the second star is and the rotor windings are shorted. Figure 1 shows the distribution of fluxes axis of all windings.

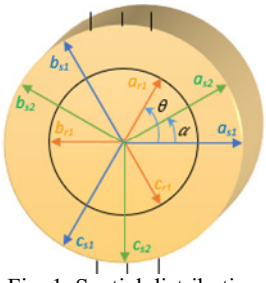

Fig. 1. Spatial distribution of fluxes in the DSIM

By applying the Park transformation on the 3 windings of the DSIM, the system will be expressed as follows [3]:

$$\begin{cases} V_{ds1} = R_s i_{ds1} + \dfrac{\mathrm{d}\phi_{ds1}}{\mathrm{d}t} - \omega_s \phi_{qs1}; \\ V_{ds2} = R_s i_{ds2} + \dfrac{\mathrm{d}\phi_{ds2}}{\mathrm{d}t} - \omega_s \phi_{qs2}; \\ V_{qs1} = R_s i_{qs1} + \dfrac{\mathrm{d}\phi_{qs1}}{\mathrm{d}t} + \omega_s \phi_{ds1}; \\ V_{qs2} = R_s i_{qs2} + \dfrac{\mathrm{d}\phi_{qs2}}{\mathrm{d}t} + \omega_s \phi_{ds2}; \\ 0 = R_r i_{dr} + \dfrac{\mathrm{d}\phi_{qs1}}{\mathrm{d}t} - (\omega_s - \omega)\phi_{ds1}; \\ 0 = R_r i_{dr} + \dfrac{\mathrm{d}\phi_{qs1}}{\mathrm{d}t} - (\omega_s - \omega)\phi_{ds1}, \end{cases} \quad (1)$$

where R_{s1}, R_{s2} are the resistances of the 1st and 2nd star; R_r is the rotor resistance; ω_s, ω are the angular velocities of the stator and the rotor; $V_{d,q(s,r)1,2}$, $i_{d,q(s,r)1,2}$, $\phi_{d,q(s,r)1,2}$ are the motor's voltages, currents and fluxes.

The stator fluxes expressions are given by:

$$\begin{cases} \phi_{ds1} = L_{s1} i_{ds1} + L_m (i_{ds1} + i_{ds2} + i_{dr}); \\ \phi_{ds2} = L_{s2} i_{ds2} + L_m (i_{ds1} + i_{ds2} + i_{dr}); \\ \phi_{qs1} = L_{s1} i_{qs1} + L_m (i_{qs1} + i_{qs2} + i_{qr}); \\ \phi_{qs2} = L_{s2} i_{qs2} + L_m (i_{qs1} + i_{qs2} + i_{qr}); \\ \phi_{dr} = L_r i_{dr} + L_m (i_{dr} + i_{ds1} + i_{ds2}); \\ \phi_{qr} = L_r i_{qr} + L_m (i_{qr} + i_{qs1} + i_{qs2}), \end{cases} \quad (2)$$

where L_{s1}, L_{s2} are the inductances of the 1st and 2nd star; L_r is the rotor inductance; L_m is the mutual inductance.

Using stator currents and rotor flux components, the equation for electromagnetic torque is:

$$T_{em} = p \frac{L_m}{L_r + L_m} (\phi_{dr}(i_{sq1} + i_{sq2}) - \phi_{qr}(i_{sd1} + i_{sd2})), \quad (3)$$

where p is the number of pole pairs.

Finally, the rotational equation is given by:

$$\frac{\mathrm{d}}{\mathrm{d}t}\Omega = \frac{1}{J}(T_{em} - T_L - F_r \Omega), \quad (4)$$

where Ω is the mechanical rotor speed; J is the moment of inertia; T_L is the load torque; F_r is the friction coefficient.

Modeling of the IFOC. The principle of field-oriented control is to realize decoupling between the magnetic flux and the torque. Unlike the direct approach, IFOC calculates the rotor flux angle indirectly by using the shafts' speed information, which eliminates the need to directly measure the rotor flux position.

By aligning the d-axis with the rotor's flux, the orientation is achieved, resulting in the following [23]:

$$\phi_{qr} = 0 \rightarrow \phi_{dr} = \phi_r. \quad (5)$$

The new system can now be governed using the decoupling terms v^*_{ds1} and e_{ds1} as follows:

$$\begin{cases} V^*_{ds1} = v^*_{ds1} + e_{ds1}; \quad V^*_{ds2} = v^*_{ds2} + e_{ds2}; \\ V^*_{qs1} = v^*_{qs1} + e_{qs1}; \quad V^*_{qs2} = v^*_{qs2} + e_{qs2}, \end{cases} \quad (6)$$

where:

$$\begin{cases} v^*_{ds1} = R_{s1} i_{ds1} + L_{s1} \dfrac{\mathrm{d}i_{ds1}}{\mathrm{d}t}; \quad v^*_{ds2} = R_{s1} i_{ds2} + L_{s1} \dfrac{\mathrm{d}i_{ds2}}{\mathrm{d}t}; \\ v^*_{qs1} = R_{s1} i_{qs1} + L_{s1} \dfrac{\mathrm{d}i_{qs1}}{\mathrm{d}t}; \quad v^*_{qs2} = R_{s1} i_{qs2} + L_{s1} \dfrac{\mathrm{d}i_{qs2}}{\mathrm{d}t}, \end{cases} \quad (7)$$

and:

$$\begin{cases} e_{ds1} = \omega_s (L_{s1} i_{qs1} + \tau_r \phi^*_r \omega_{sl}); \; e_{ds2} = \omega_s (L_{s2} i_{qs2} + \tau_r \phi^*_r \omega_{sl}); \\ e_{qs1} = \omega_s (L_{s1} i_{ds1} + \phi^*_r); \; e_{qs2} = \omega_s (L_{s2} i_{ds2} + \phi^*_r), \end{cases} \quad (8)$$

where $\tau_r = L_r/R_r$ is the rotor time constant; ω_{sl} is the slip frequency. The symbol (*) indicates the references.

The electromagnetic torque is:

$$T_{em} = p \frac{L_m}{L_r + L_m} (\phi^*_{dr}(i_{sq1} + i_{sq2})) = p \frac{L_m}{L_r + L_m} \phi^*_{dr} i^*_{sq}), \quad (9)$$

Equation (9) shows that the electromagnetic torque is similar to that of a separately excited DC motor, which demonstrates that torque and flux are now decoupled.

The synchronous angular speed can be derived as:

$$\omega_s = \omega + \omega_{sl} = p\Omega + \frac{L_m R_r}{L_m + L_r}\frac{i_{qs}^*}{\phi_{dr}^*}, \qquad (10)$$

The complete scheme of the classical PI-based IFOC is presented in Fig. 2.

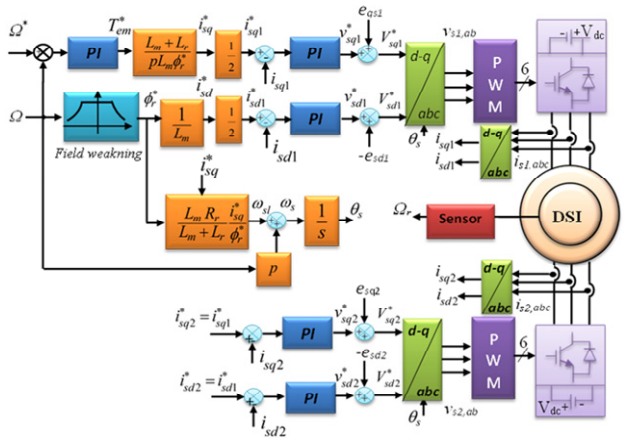

Fig. 2. Schematic of the classical IFOC with PI-based controllers fed by double 2-levels inverters

Design of the LQR. In this section, the LQR will be used as an advanced regulator to regulate speed and torque of the DSIM, in objective to ensure high robustness against phase fault, load torque variation, high precision within the shortest time possible without surpassing the motor capacity.

First, let's take the Laplace transform of (4) considering T_L as perturbation (i.e. $T_L = 0$) as follows:

$$\frac{\Omega}{T_{em}} = \frac{1}{Js + F_r}. \qquad (11)$$

To define the LQR regulator, (11) must be converted into state-space representation. For this purpose, state-space variables are chosen so that:

$$\begin{cases} x_1 = \Omega; \\ x_2 = \dot{\Omega}, \end{cases} \qquad (12)$$

Using (4) in (12) will give:

$$\begin{cases} \dot{x}_1 = x_2; \\ x_2 = 1/J = (T_{em} - T_L - F_r x_1). \end{cases} \qquad (13)$$

In matrix form it will be:

$$\begin{bmatrix} \dot{x}_1 \\ \dot{x}_2 \end{bmatrix} = \begin{bmatrix} 0 & 1 \\ -F_r/J & 0 \end{bmatrix}\begin{bmatrix} x_1 \\ x_2 \end{bmatrix} + \begin{bmatrix} 0 \\ 1 \end{bmatrix} T_{em} - \begin{bmatrix} 0 \\ 1/J \end{bmatrix} T_L. \qquad (14)$$

The output of this system is:

$$y = \begin{bmatrix} 1 & 0 \end{bmatrix}\begin{bmatrix} x_1 \\ x_2 \end{bmatrix}. \qquad (15)$$

So, the matrixes A, B, C, D are then defined as:

$$[A] = \begin{bmatrix} 0 & 1 \\ -F_r/J & 0 \end{bmatrix}, [B] = \begin{bmatrix} 0 \\ 1 \end{bmatrix}, [C] = \begin{bmatrix} 1 & 0 \end{bmatrix}, [D] = 0.$$

The control law of the LQR regulator is defined as:

$$U_{lqr} = -K_{lqr}[x]. \qquad (16)$$

where K_{lqr} is the feedback gain of the regulator:

$$K_{lqr} = R \cdot B \cdot P, \qquad (17)$$

where R is the 1st controller matrix. In our case it has been set as:

$$R = 5\begin{bmatrix} -50 & 50 \\ 1 & -50 \end{bmatrix};$$

P is the solution of the covariance equation (Ricatti equation) which is defined by:

$$A^T \cdot P + P \cdot A - P \cdot B \cdot R^{-1} \cdot B^T \cdot P + C^T \cdot Q \cdot C = 0. \qquad (18)$$

Q is the 2nd controller matrix: $Q = 100$.

The matrixes R and Q represent a degree of freedom to adjust between minimization of the error and the effort of the control, in other way to control precision and response speed. The only inconvenient of this technique is to find a relationship between these 2 matrixes to ensure the desired robustness.

Substituting (16) in (18) will lead to a closed loop system such that:

$$[\dot{x}] = ([A] - [B \cdot K_{lqr}])[x]. \qquad (19)$$

The new state space of the system will be:

$$\begin{cases} [\dot{x}] = [A_{lqr}][x] \\ y = [C][x] \end{cases}. \qquad (20)$$

The structure of the LQR regulator used in the speed loop is depicted in Fig. 3.

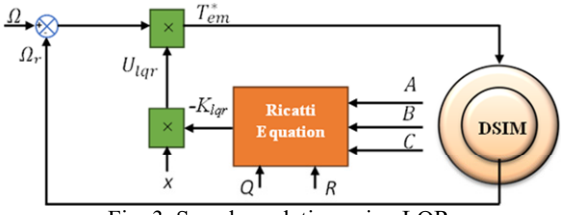

Fig. 3. Speed regulation using LQR

Modeling of the ADRC. ADRC is a robust control strategy designed to estimate and compensate for system uncertainties, external disturbances, and nonlinearities in real-time. By combining an extended state observer to estimate disturbances and a feedback controller to reject them, ADRC enhances the performance and stability of dynamic systems.

The ADRC control was first proposed by Han in 1990s as an alternative to PID controllers [24]. Since then, it has been used in flux or torque regulator in vector control [25–29]. We opted to apply it to the DSIM, in aim to improve torque response, reduce sensitivity to parameter variations, and ensure robust operation under load disturbances. The illustration of the used ADRC is shown on Fig. 4 [30].

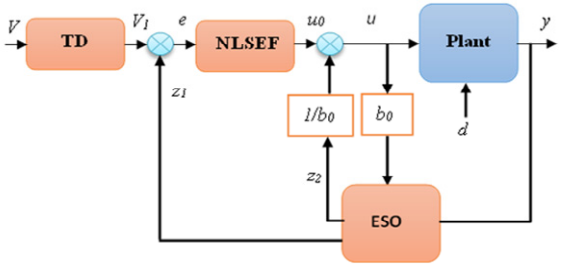

Fig. 4. Schematic description of the ADRC

According to this work, V_1 is the tracking signal for the current reference $i^*_{sdq(1,2)}$, while e is the error signal of the current loop. The term u_0 corresponds to the output of the nonlinear state error feedback, and u is the reference voltage adjusted by the estimated disturbance. Additionally, z_1 and z_2 are the tracking signal for $i_{sdq(1,2)}$

and the estimated disturbance, respectively. The tracking differentiator makes the feed-back error change gradually to solve the contradiction between rapidity and over-shoot. And b_0 is a nominal control gain, it's an estimate of the system's input gain, which relates the control input to the system's dynamics.

Thus, 4 ADRC regulators will be used to control the DSIM currents, where their outputs will constitute the input voltages of the inverters. As it can be seen in Fig. 5, based on the current transfer function of the DSIM, the state formulation of current loop can be defined by:

$$\begin{cases} x_1 = i_{s1,2(dq)}(t); \\ x_2 = \dot{i}_{s1,2(dq)}(t). \end{cases} \quad (21)$$

$$\begin{cases} \dot{x}_1 = x_2; \\ \dot{x}_2 = \dfrac{1}{L_s}\left(u(t) - R_s x_2\right). \end{cases} \quad (22)$$

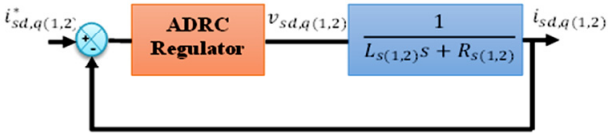

Fig. 5. Currents regulation using ADRC regulator

The current's matrixes of the system will be:

$$[A] = \begin{bmatrix} 0 & 1 \\ -R_s/L_s & 0 \end{bmatrix}, [B] = \begin{bmatrix} 0 \\ 1/L_s \end{bmatrix}, [C] = [1 \quad 0], [D] = 0.$$

The ADRC regulator will be used to compensate the last system, so the new state space will be:

$$\begin{cases} \dot{x}_1 = x_2; \\ \dot{x}_2 = 1/L_s\left(u(t - R_s x_1 + z_2(t)\right); \\ \dot{x}_3 = z_2(t). \end{cases} \quad (23)$$

The control low of the previous system shown in (23) will be:

$$\begin{cases} u_0 = \left(i_{ref} - z_1\right) w_c^2 - 2\, w_c\, z_2(t); \\ u(t) = \dfrac{1}{b_0}\left(u_0 - z_2(t)\right), \end{cases} \quad (24)$$

where $w_c = 5000$ is the bandwidth of the observer; $b_0 = 5000$.

The extended state space of the previous system shown in (23) will be:

$$[\dot{x}] = \begin{bmatrix} 0 & 1 & 0 \\ R_s/L_s & 0 & 1 \\ 0 & 0 & 0 \end{bmatrix} \begin{bmatrix} x_1 \\ x_2 \\ x_3 \end{bmatrix} + \begin{bmatrix} 0 \\ 1/L_s \\ 0 \end{bmatrix} \frac{(u_0 - z(t))}{b_0}. \quad (25)$$

While the output of the extended system is:

$$y(t) = [1 \quad 0 \quad 0] \begin{bmatrix} x_1 \\ x_2 \\ x_3 \end{bmatrix}. \quad (26)$$

And the new matrixes are:

$$[A_{ext}] = \begin{bmatrix} 0 & 1 & 0 \\ R_s/L_s & 0 & 1 \\ 0 & 0 & 0 \end{bmatrix}, B_{ext} = \begin{bmatrix} 0 \\ 1/L_s \\ 0 \end{bmatrix}, C_{ext} = [1 \quad 0 \quad 0].$$

The scheme of the proposed strategy is shown in Fig. 6.

Simulation results and discussion. In this section, we will evaluate the performance and robustness of the DSIM fed by dual 3-level neutral point clamped inverters.

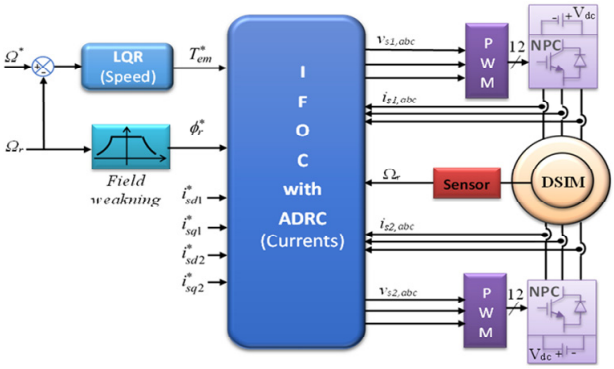

Fig. 6. Global control scheme of the proposed LQR-ADRC speed and current controllers connected to dual neutral point clamped inverters

Using MATLAB/Simulink, 2 control strategies were tested: the traditional IFOC with PI regulators, and an advanced approach combining IFOC with LQR for electromagnetic torque control and ADRC for current regulation. The simulations include tests to assess the system's ability to track speed references, handle external disturbances, and maintain stability under challenging conditions, such as phase faults and internal parameter variations. Additionally, a THD study is conducted to evaluate the system's harmonic suppression capabilities. The motor parameters used in this study are listed in Table 1 [31].

Table 1

DSIM parameters

Parameters	Value
Rated power P, kW	4.5
Line-to-line voltage V_n, V	380
Rated speed Ω_n, rad/s	288.29
Number of pole pairs p	1
Stator inductance L_s, mH	22
Rotor inductance L_r, mH	6
Mutual inductance L_m, H	0.4092
Stator resistance R_s, Ω	3.72
Rotor resistance R_r, Ω	2.12
Moment of inertia J, kg·m^2	0.00625
Friction coefficient F_r, m/(rad·s^{-1})	0.001

Test 1. *Evaluation of reference tracking at variable speed.* Figures 7, 8 illustrate the speed and torque responses of the DSIM controlled by the classical IFOC (Ω_{PI}, $T_{em(PI)}$) and the IFOC-based LQR-ADRC approach ($\Omega_{LQR\text{-}ADRC}$, $T_{em(LQR\text{-}ADRC)}$) under varying speed references. Initially, the motor operates with a speed reference of 100 rad/s, 300 rad/s, followed by a reduction to 200 rad/s, and finally reverses its rotation to –100 rad/s. These figures demonstrate the system's ability to track both positive and negative speed references with minimal delay, indicating robust and efficient speed control. At start, it's shown that the torque peak is the same for both techniques (≈56 N·m). After that, the variation in the speed reference causes transient scenarios in torque for both techniques. However, the LQR-ADRC demonstrates a faster stabilization time, with the presence of additional peaks ≈20 N·m, while the IFOC-PI shows a longer stabilization time with less peaks and torque ripples.

Figures 9, 10 show the direct and quadrature components of the flux (ϕ_{dr}, ϕ_{qr}) of the DSIM. It can be seen that the orientations are successfully achieved. However, the LQR-ADRC shows a stable decoupling

despite some ripples at speed reference changing, while the classical IFOC shows a longer and stable response.

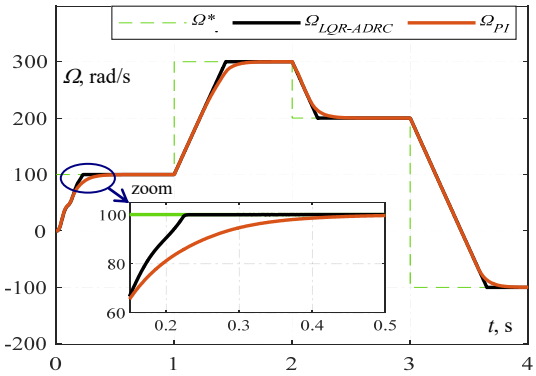

Fig. 7. Speed of the DSIM under variable speed reference

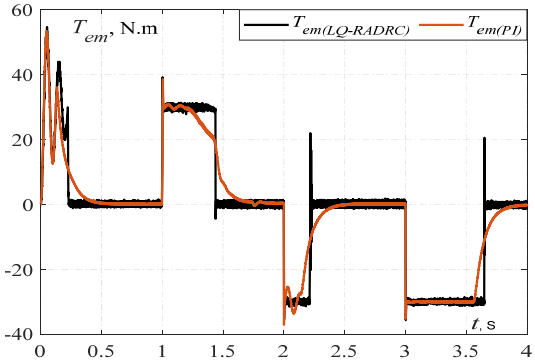

Fig. 8. Torque of the DSIM under variable speed reference

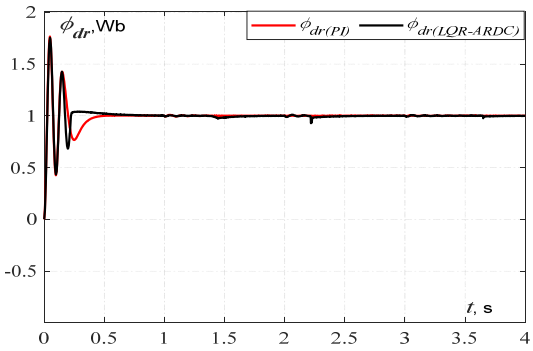

Fig. 9. PI and LQR-ADRC direct flux ϕ_{dr} components

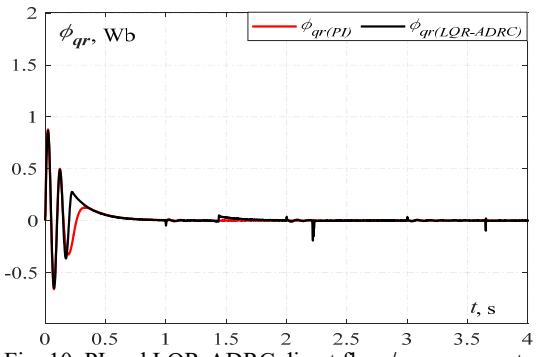

Fig. 10. PI and LQR-ADRC direct flux ϕ_{qr} components

Table 2 compares the 2 approaches in terms of stabilization time, overshoot, and precision. One can observe that the new approach (LQR-ADRC-based IFOC) surpasses the classical PI-IFOC in both precision and stabilization time, while maintaining 0 % overshoot. This demonstrates high robustness in tracking reference speeds.

Table 2

PI-based vs LQR-ADRC-based IFOC performance analysis

Criteria	Speed range, rad/s	Classical IFOC	LQR-ADRC based IFOC
Stabilizing t, s	0→100	0.5	0.24
	100→300	0.7	0.4
	300→200	0.45	0.25
	200→ –100	1	0.65
Overshoot, %		0	0
Precision, %		99	99.98

Test 2. *Performance against external disturbance.* Here, the motor starts with 250 rad/s step reference. Then, a sequence of multiple load-torques are applied as the following: T_L=10 N·m at t = 1 s, T_L=20 N·m at t = 2 s, and T_L= –20 N·m at t = 3 s. From Fig. 11, the LQR-ADRC instantly rejects disturbances, while the PI-based IFOC has significantly longer rejection time. Figure 12 shows the LQR-ADRC's electromagnetic torque response is faster than classical IFOC.

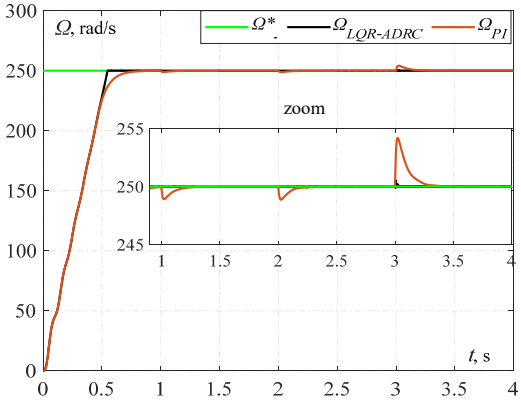

Fig. 11. Speed of the DSIM under load variation

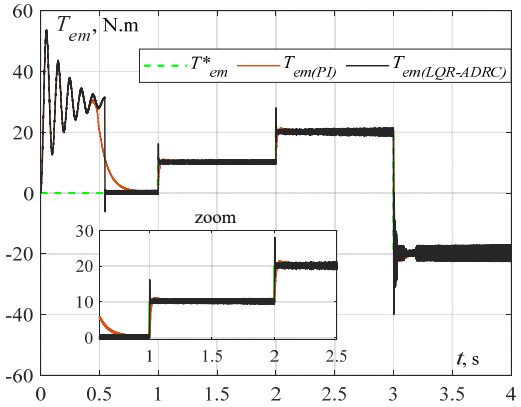

Fig. 12. Torque of the DSIM under load variation

Test 3. *THD comparison*. Figures 13, 14 show the currents of the 1st star of the DSMI. The waves form is regular in LQR-ADRC compared to classic IFOC.

Figures 15, 16 reveal a THD of 13.72 % with PI-based IFOC, compared to 5.18 % with LQR-ADRC-based IFOC. This demonstrates that the proposed approach is more effective at minimizing harmonics.

Following the 3 tests and the analysis of their results, which demonstrate that the LQR-ADRC outperforms the IFOC in most scenarios, further tests will be conducted to evaluate the robustness of this new approach. This time, the focus will be on phase faults and internal disturbances, such as variations in stator and rotor resistances and changes in the moment of inertia.

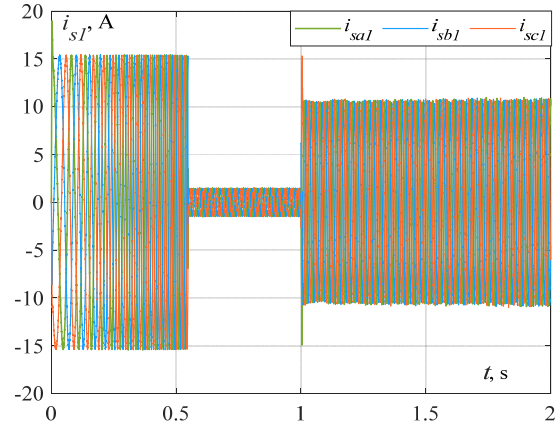

Fig. 13. Currents of the 1st star controlled by LQR-ADRC

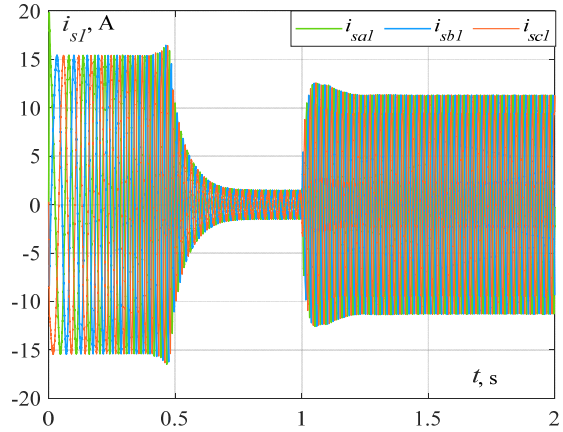

Fig. 14. Currents of the 1st star controlled by IFOC-PI

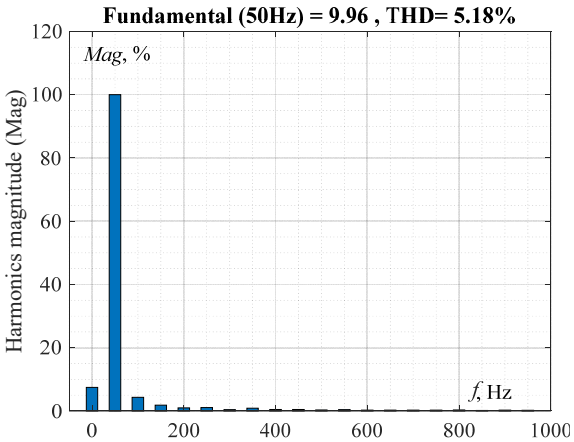

Fig. 15. THD of i_{sa1} controlled by LQR-ADRC

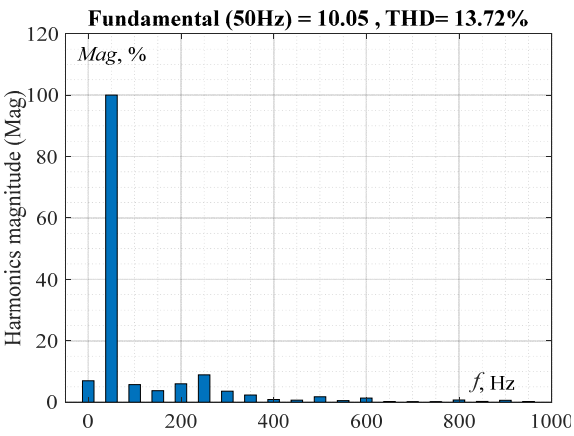

Fig. 16. THD of i_{sa1} controlled by IFOC-PI

Test 4. *Phase fault examination*. In this test, the motor will start with a load torque T_L=20 N·m. It will then encounter several changes of reference speed and at t = 4 s, a phase fault will occur in the phase A of the 1st star. Figure 17 represents the speed response of the DSIM, while Fig. 18 shows the electromagnetic torque. Despite these severe conditions, the system continues to operate effectively without losing service continuity or compromising its stability. It demonstrates remarkable resilience, maintaining its robustness and consistent performance even under challenging circumstances.

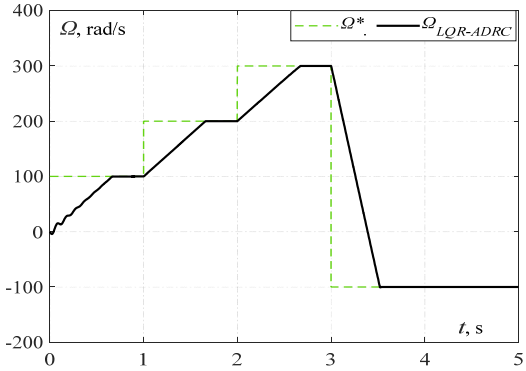

Fig. 17. Speed of the DSIM under variable speed, load torque and phase fault

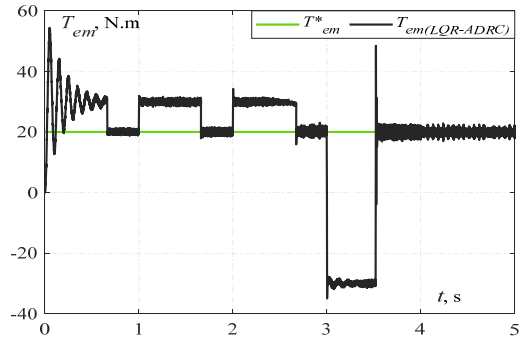

Fig. 18. Torque of the DSIM under variable speed, load torque and phase fault

Test 5. *Robustness against internal parameters changing*. The impact of parameters variation is a critical factor in the performance of the control system. These changes can affect the dynamics of the motor such as the rotor flux linkage, torque production, and current regulation.

At this scenario, tests will be conducted against internal parameters such as R_s, R_r and J to evaluate the system's robustness. First the system will start with normal parameters. In all scenarios, the motor will operate at a reference speed of 100 rad/s, with a resistant torque of 20 N·m applied at t = 1 s. The parameter will then be multiplied by 1.5 at t = 2 s, by 2 at t = 3 s, and by 2.5 at t = 4 s, resulting in a 250 % increase.

Figures 19–24 highlight that rotor resistance variations influence the transient dynamics without compromising the stability or balance of the stator currents thanks to the proposed controllers. Despite these variations, the control system maintains robust performance, as evidenced by the actual speed consistently aligning with the reference speed without noticeable deviations or delays. This indicates that the control strategy effectively compensates for the effects of resistance changes, ensuring stability and precision.

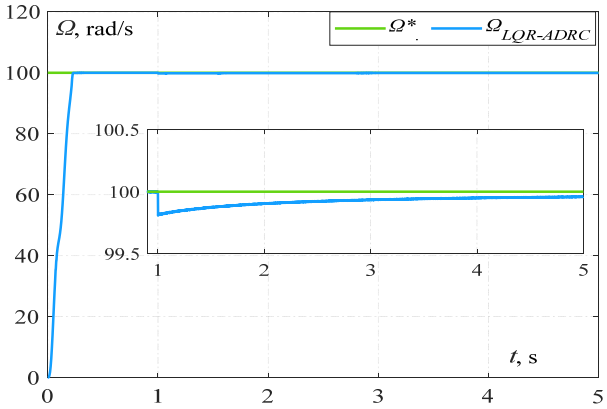

Fig. 19. Speed of the DSIM under stator resistance variation

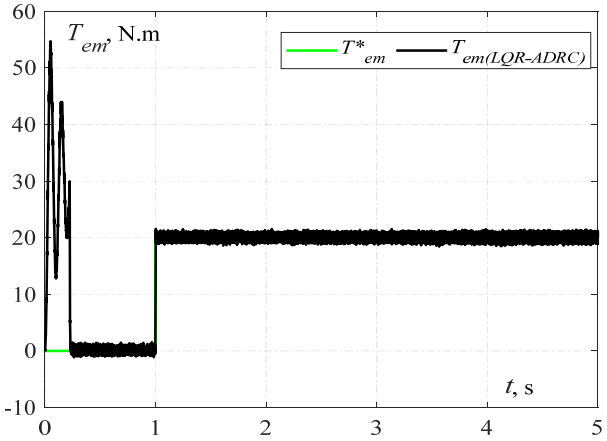

Fig. 20. Torque of the DSIM under stator resistance variation

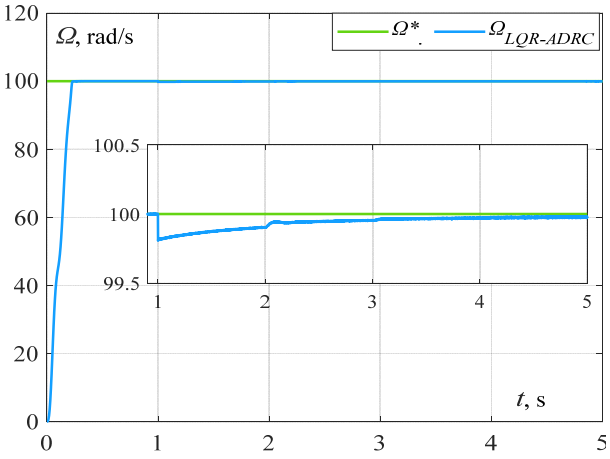

Fig. 21. Speed of the DSIM under rotor resistance variation

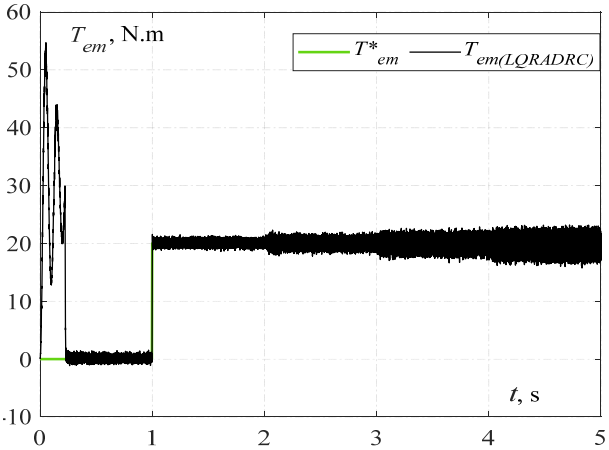

Fig. 22. Torque of the DSIM under rotor resistance variation

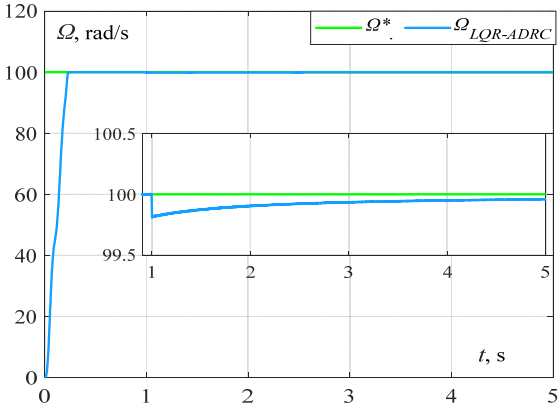

Fig. 23. Speed of the DSIM under inertia variation

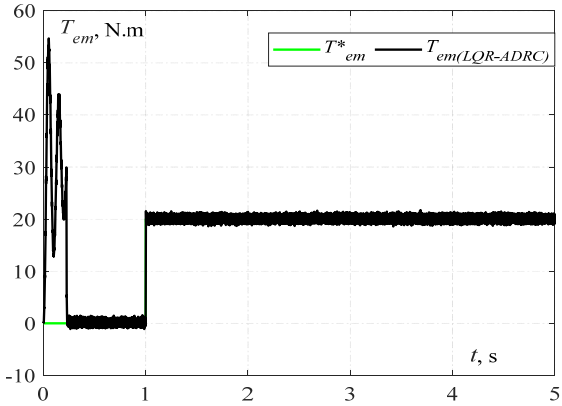

Fig. 24. Torque of the DSIM under moment of inertia variation

Conclusions. In this work, LQR regulator has been employed to regulate the speed of a DSIM, while ADRC regulators have been used to control the currents.

Several tests have been conducted and the results revealed that the LQR-ADRC-based IFOC control strategy significantly outperforms the classical PI-IFOC in terms of speed control, stabilization time, and robustness. The LQR-ADRC exhibits faster stabilization times across various speed transitions, with minimal current ripples and no overshoot, maintaining a high precision. It also shows superior performance under external disturbances, such as load torque variations, where it maintains speed response stability without significant deviations. In phase fault scenarios and internal parameter variations, the LQR-ADRC proves highly robust, maintaining precise speed control and stability even under degraded conditions. In conclusion, the LQR-ADRC-based IFOC emerges as a more efficient and robust control strategy, particularly in dynamic and challenging operational conditions.

Conflict of interest. The authors declare that they have no conflicts of interest.

REFERENCES

1. Volkov V.A., Antonov N.L. Refined calculation of energy modes of a frequency-regulated induction motor. *Electrical Engineering & Electromechanics*, 2024, no. 5, pp. 3-13. doi: https://doi.org/10.20998/2074-272X.2024.5.01.

2. Chaib Ras A., Bouzerara R., Bouzeria H. An adaptive controller for power quality control in high speed railway with electric locomotives with asynchronous traction motors. *Electrical Engineering & Electromechanics*, 2024, no. 2, pp. 23-30. doi: https://doi.org/10.20998/2074-272X.2024.2.04.

3. Salem A., Narimani M. A Review on Multiphase Drives for Automotive Traction Applications. *IEEE Transactions on Transportation Electrification*, 2019, vol. 5, no. 4, pp. 1329-1348. doi: https://doi.org/10.1109/TTE.2019.2956355.

4. Rinkeviciene R., Savickiene Z., Uznys D., Pitrenas A., Slepikas A. Scalar control of six-phase induction motor. *2017 Open Conference of Electrical, Electronic and Information Sciences (EStream)*, 2017, pp. 1-6. doi: https://doi.org/10.1109/eStream.2017.7950304.
5. Mossa M.A., Khouidmi H., Ma'arif A. Robust Flux and Speed State Observer Design for Sensorless Control of a Double Star Induction Motor. *Journal of Robotics and Control (JRC)*, 2022, vol. 3, no. 4, pp. 464-475. doi: https://doi.org/10.18196/jrc.v3i4.15667.
6. Chatterjee S., Chatterjee S. A novel speed sensor-less vector control of Dual Stator Induction machine with space vector based advanced 9-zone hybrid PWM for grid connected wind energy generation system. *Electric Power Systems Research*, 2018, vol. 163, pp. 174-195. doi: https://doi.org/10.1016/j.epsr.2018.02.021.
7. Pandit J.K., Aware M.V., Nemade R., Tatte Y. Simplified Implementation of Synthetic Vectors for DTC of Asymmetric Six-Phase Induction Motor Drives. *IEEE Transactions on Industry Applications*, 2018, vol. 54, no. 3, pp. 2306-2318. doi: https://doi.org/10.1109/TIA.2018.2789858.
8. Guedida S., Tabbache B., Nounou K., Benbouzid M. Direct torque control scheme for less harmonic currents and torque ripples for dual star induction motor. *Revue Roumaine des Sciences Techniques – Série Électrotechnique et Énergétique*, 2023, vol. 68, no. 4, pp. 331-338. doi: https://doi.org/10.59277/RRST-EE.2023.4.2.
9. Ayaz Khoshhava M., Abootorabi Zarchi H., Markadeh G. Sensor-less Speed and Flux Control of Dual Stator Winding Induction Motors Based on Super Twisting Sliding Mode Control. *IEEE Transactions on Energy Conversion*, 2021, vol. 36, no. 4, pp. 3231-3240. doi: https://doi.org/10.1109/TEC.2021.3077829.
10. Abdallah A., Bouchetta A., Boughazi O., Baghdadi A., Bousserhane L.K. Double star induction machine using nonlinear integral backstepping control. *International Journal of Power Electronics and Drive Systems (IJPEDS)*, 2019, vol. 10, no. 1, pp. 27-40. doi: https://doi.org/10.11591/ijpeds.v10.i1.pp27-40.
11. Nemouchi B., Rezgui S.E., Benalla H., Nebti K. Fractional-based iterative learning-optimal model predictive control of speed induction motor regulation for electric vehicles application. *Electrical Engineering & Electromechanics*, 2024, no. 5, pp. 14-19. doi: https://doi.org/10.20998/2074-272X.2024.5.02.
12. Babes B., Hamouda N., Kahla S., Amar H., Ghoneim S.S.M. Fuzzy model based multivariable predictive control design for rapid and efficient speed-sensorless maximum power extraction of renewable wind generators. *Electrical Engineering & Electromechanics*, 2022, no. 3, pp. 51-62. doi: https://doi.org/10.20998/2074-272X.2022.3.08.
13. Gonzalez O., Ayala M., Romero C., Delorme L., Rodas J., Gregor R., Gonzalez-Prieto I., Duran M.J. Model Predictive Current Control of Six-Phase Induction Motor Drives Using Virtual Vectors and Space Vector Modulation. *IEEE Transactions on Power Electronics*, 2022, vol. 37, no. 7, pp. 7617-7628. doi: https://doi.org/10.1109/TPEL.2022.3141405.
14. Hadji C., Khodja D., Chakroune S. Robust Adaptive Control of Dual Star Asynchronous Machine by Reference Model Based on Landau Stability Theorem. *Advances in Modelling and Analysis C*, 2019, vol. 74, no. 2-4, pp. 56-62. doi: https://doi.org/10.18280/ama_c.742-403.
15. Youb L., Belkacem S., Naceri F., Cernat M., Pesquer L.G. Design of an Adaptive Fuzzy Control System for Dual Star Induction Motor Drives. *Advances in Electrical and Computer Engineering*, 2018, vol. 18, no. 3, pp. 37-44. doi: https://doi.org/10.4316/AECE.2018.03006.
16. Lazreg M.H., Bentaallah. A. Sensorless Speed Control of Double Star Induction Machine With Five Level DTC Exploiting Neural Network and Extended Kalman Filter. *Iranian Journal of Electrical and Electronic Engineering*, 2019, vol. 15, no. 1, pp. 142-150. doi: http://doi.org/10.22068/IJEEE.15.1.142.
17. Bentouhami L., Abdessemed R., Kessal A., Merabet E. Control Neuro-Fuzzy of a Dual Star Induction Machine (DSIM) supplied by Five-Level Inverter. *Journal of Power Technologies*, 2018, vol. 98, no. 1, pp. 70-79.
18. Guermit H., Kouzi K., Bessedik S.A. Novel design of an optimized synergetic control for dual stator induction motor. *COMPEL - The International Journal for Computation and Mathematics in Electrical and Electronic Engineering*, 2019, vol. 38, no. 6, pp. 1828-1845. doi: https://doi.org/10.1108/COMPEL-01-2019-0042.
19. Ebrahim O.S., Salem M.F., Jain P.K., Badr M.A. Application of linear quadratic regulator theory to the stator field-oriented control of induction motors. *IET Electric Power Applications*, 2010, vol. 4, no. 8, pp. 637-646. doi: https://doi.org/10.1049/iet-epa.2009.0164.
20. Swargiary M., Dey J., Saha T.K. Optimal speed control of induction motor based on Linear Quadratic Regulator theory. *2015 Annual IEEE India Conference (INDICON)*, 2015, pp. 1-6. doi: https://doi.org/10.1109/INDICON.2015.7443806.
21. Janous S., Talla J., Smidl V., Peroutka Z. Constrained LQR Control of Dual Induction Motor Single Inverter Drive. *IEEE Transactions on Industrial Electronics*, 2021, vol. 68, no. 7, pp. 5548-5558. doi: https://doi.org/10.1109/TIE.2020.2994885.
22. Oumar A., Ahmed Y., Cherkaoui M. Operating of DSIM without current and speed sensors controlled by ADRC control. *Mathematical Problems in Engineering*, 2022, pp. 1-8. doi: https://doi.org/10.1155/2022/9033780.
23. Khemis A., Boutabba T., Drid S. Model reference adaptive system speed estimator based on type-1 and type-2 fuzzy logic sensorless control of electrical vehicle with electrical differential. *Electrical Engineering & Electromechanics*, 2023, no. 4, pp. 19-25. doi: https://doi.org/10.20998/2074-272X.2023.4.03.
24. Huang Y., Xue W., Zhiqiang G., Sira-Ramirez H., Wu D., Sun M. Active disturbance rejection control: Methodology, practice and analysis. *Proceedings of the 33rd Chinese Control Conference*, 2014, pp. 1-5. doi: https://doi.org/10.1109/ChiCC.2014.6896585.
25. Kelam S. Nonlinear robust ADRC control of induction machine. *Przegląd Elektrotechniczny*, 2023, no. 3, pp. 211-217. doi: https://doi.org/10.15199/48.2023.03.37.
26. Chalawane H., Essadki A., Nasser T., Arbaoui M. A new robust control based on active disturbance rejection controller for speed sensorless induction motor. *2017 International Conference on Electrical and Information Technologies (ICEIT)*, 2017, pp. 1-6. doi: https://doi.org/10.1109/EITech.2017.8255226.
27. Oumar A., Chakib R., Cherkaoui M. Current Sensor Fault-Tolerant Control of DSIM Controlled by ADRC. *Mathematical Problems in Engineering*, 2020, art. no. 6568297. doi: https://doi.org/10.1155/2020/6568297.
28. Hezzi A., Ben Elghali S., Bensalem Y., Zhou Z., Benbouzid M., Abdelkrim M.N. ADRC-Based Robust and Resilient Control of a 5-Phase PMSM Driven Electric Vehicle. *Machines*, 2020, vol. 8, no. 2, art. no. 17. doi: https://doi.org/10.3390/machines8020017.
29. Vinh V.Q., Phat T.C., Giang N.H. An Adaptive Active Disturbance Rejection Controller (ADRC) for Induction Motor Drives. *International Journal of Electrical and Electronics Engineering*, 2024, vol. 11, no. 12, pp. 295-301. doi: https://doi.org/10.14445/23488379/IJEEE-V11I12P127.
30. Han J. From PID to Active Disturbance Rejection Control. *IEEE Transactions on Industrial Electronics*, 2009, vol. 56, no. 3, pp. 900-906. doi: https://doi.org/10.1109/TIE.2008.2011621.
31. Darsouni Z., Rezgui S.E., Benalla H., Rebahi F., Boumendjel M.A.M. Ensuring service continuity in electric vehicles with vector control and linear quadratic regulator for dual star induction motors. *Electrical Engineering & Electromechanics*, 2025, no. 2, pp. 24-30. doi: https://doi.org/10.20998/2074-272X.2025.2.04.

Received 13.03.2025
Accepted 18.05.2025
Published 02.11.2025

S.E. Rezgui[1], *Doctor of Technical Sciences, Associate Professor,*
Z. Darsouni[1], *PhD Student,*
H. Benalla[1], *Full Professor,*
[1] Laboratory of Electrical Engineering of Constantine (LEC),
Technology Sciences Faculty,
University Constantine 1 Freres Mentouri, Algeria,
e-mail: rezgui.salaheddine@umc.edu.dz (Corresponding Author);
darsounizakaria@gmail.com; benalla.hocine@umc.edu.dz

How to cite this article:
Rezgui S.E., Darsouni Z., Benalla H. Nonlinear vector control of multiphase induction motor using linear quadratic regulator and active disturbances rejection control under disturbances and parameter variations. *Electrical Engineering & Electromechanics*, 2025, no. 6, pp. 75-83. doi: https://doi.org/10.20998/2074-272X.2025.6.10